JOURNAL OF MATERIALS SCIENCE 17 (1982) 717–731

Microstructural investigation of a Co-base alloy processed by liquid phase sintering

C. GUYARD, S. HAMAR-THIBAULT, C. H. ALLIBERT
Institut National Polytechnique de Grenoble, Laboratoire de Thermodynamique et Physico-Chimie Métallurgiques (L.A. 29), E.N.S.E.E.G., Domaine Universitaire B.P. 44, 38401 Saint Martin d'Hères, France

The microstructure of samples processed by liquid phase sintering of prealloyed atomized powders is investigated by microprobe analysis, X-ray and electron diffraction. Materials obtained from thin powders are shown to consist of a dispersion of M_7C_3 in a Co matrix; the composition of the phases corresponds to the thermodynamic equilibria. A coarser powder provides a cellular structure containing islands of very thin spheroidal structure as well as M_7C_3 and a Co matrix. The W level is very high in these islands (star phase). A comparison of compositions indicates these islands correspond to the massive solidification of the undercooled liquid phase strongly saturated in W, Cr and C. For all the samples, during ageing, intense precipitation of $M_{23}C_6$ occurs in coherency with the Co matrix. The structure of the star phase coarsens and the W level decreases. After long ageing the star phase consists of only M_7C_3 and a Co matrix.

1. Introduction

Cobalt-base alloys are extensively used as hard-facing alloys owing to their good resistance to wear, hot corrosion or erosion. The best known of these alloys is stellite 6 which contains mainly Co, Cr, W and C; it is generally produced for the different weld surfacing processes, such as gas and arc-welding techniques. As shown by several authors [1, 2], the deposits obtained consist of a dendritic microstructure in which the large dendrites of a face-centred cubic (fcc) Co phase are surrounded by a eutectic mixture of M_7C_3 carbide and f c c solid solution. The composition of the phases solidified in the weld deposits was determined by Silence [3]; it corresponds roughly with that measured in equilibrium conditions by Guyard *et al.* [4].

According to Hickl [2], the strength of this material can be attributed to the combination of the highly alloyed f c c matrix and hard stable carbides. Silence [3] found that the abrasion resistance increased with the carbon content of the alloys and was controlled by the volume-fraction and size of the carbides. Referring to the microstructure produced by weld-deposit or solidification, the rather large size of the carbide does not promote any great enhancement of abrasion resistance; better results could be expected from a material with a higher dispersion of thinner carbides. The coarse dendritic structure of solidification mainly results from the broad interval between the liquidus and solidus temperatures of this alloy which were located at about 1360 and 1260° C by Guyard *et al.* [4]. The improvement of such a microstructure requires a preparation process which avoids the complete melting of the alloy. The availability of prealloyed powders, currently prepared by inert gas atomization, suggests that liquid phase sintering would be an efficient way to obtain a fine dispersion of carbides in a f c c matrix.

In this special case, sintering proceeds from the amount of liquid phase produced by the partial melting of the alloy when heated above the solidus temperature. The microstructure so-formed is mainly related to the volume-fraction and distribution of the liquid phase involved. For a well-defined volume-fraction, the distribution of the liquid phase is strongly dependent on the grain size of the powder. In a previous study, Guyard *et al.* [5] determined the effect of the main

0022–2461/82/030717–15$04.30/0

parameters on the shrinkage of the material: results indicate almost complete densification (99.5%) to be obtained by sintering the powders at 1295° C when a molten fraction of about 40 vol% is present. The present investigation concerns the microstructural study of materials obtained after sintering of two grain size ranges of prealloyed powders of PY 250* under the same heating conditions (time, temperature, atmosphere). The effect of ageing treatments at several temperatures is also studied.

2. Experimental procedure

2.1. Preparation of samples

The powders were funnelled into small alumina crucibles, without any previous compaction. The two crucibles, containing the two different grain size ranges, were heated simultaneously up to 1295° C in 40 min. The sintering period, at 1295° C, was 60 min long, and was followed by rapid cooling. All experiments were performed under vacuum (10^{-6} torr); it was found that the impurity of the atmosphere was very important as any trace of moisture might produce partial decarburization of the alloy. For the two grain size powders, microstructures produced by the same heating treatment were very different. Grain size and composition of the starting material are given in Table I.

Ageing of the two types of samples were performed in the same furnace for 2 h at 900° C, 4 h at 1150° C and 4 h at 1230° C.

2.2. Microstructural investigation methods

2.2.1. Microstructure

At room temperature, microstructure was observed by optical microscopy of polished samples after chemical or electrolytic ethcing. The Murakami reagent (30 g Potassium Ferricyanide, 30 g Potassium Hydroxide and 60 ml water) was chosen as a chemical etchant, Struers A_2 electrolyte was used for electrolytic etching.

For high magnification, photoemission electron microscopy (with a Balzers KE 3 Metioscope) and scanning electron microscopy, SEM, (with a JEOL 5) gave good results on bulk unetched samples. Some high temperature *in situ* observations were effected, up to 900° C, in this case heating rates were very slow.

2.2.2. Phase composition analysis

When their size was large enough, the composition of the several phases was determined with an electron microprobe Cameca MS 46. For Co, Cr, W and Fe, the intensities of the Kα radiations were measured using an accelerating voltage of 20 kV. For C and Si, the Kα radiation intensities were counted with 10 and 6 kV voltages. Due to the different accelerating voltages used, all of the elements cannot be analysed at the same time. In order to minimize the errors due to this fact, all of the samples to be measured were embedded together in such a way that each element could be analysed simultaneously and exactly under the same conditions for all the samples. Consequently a comparison of the content of the main elements in each phase can be obtained accurately. The measured values of composition were corrected by a computer program taking into account the effects of atomic number, Z, absorption, A, and fluorescence, F.

For most of the elements (Co, Cr, W, Fe), the analysis conditions were good but this was not the case for the analysis of C in the f c c phase. As the C content was very low, the accuracy of the C analysis was very poor. In order to get better precision, synthetic samples containing 60 and 300 ppm of C were prepared and used as standards; despite this, the measurements always gave the same limit value and it was never possible to detect any variation of the C level in the f c c phase. In the carbides, due to the high C level, C (diamond) was chosen as a pure standard and the accuracy of the measurements could be estimated to within ± 0.5 wt %.

In the materials studied, some microstructures

TABLE I Composition and grain size of the starting material

Size	Content	C	Si	Fe	Cr	Co	W	O	N
< 36 μm	weight %	1.17	1.09	0.26	28.59	64.20	4.69	220 ppm	587 ppm
	atomic %	5.40	2.15	0.26	30.45	60.34	1.4		
< 500 μm	weight %	1.16	1.06	0.28	28.63	64.02	4.85	100 ppm	681 ppm
	atomic %	5.36	2.09	0.28	30.54	60.26	1.46		

*PY 250 is a registered trademark of Imphy SA.

observed were too thin for each constitutive phase to be analysed. In this case, the mean composition value was measured by using an unfocussed microprobe (8 to 10 μm).

2.2.3. Crystal structures

The crystal structure of the several phases was determined by X-ray and electron diffractions.

Due to the rather low proportion of precipitated carbides in the samples, X-ray diffraction on bulk or powdered materials did not give unambiguous results. Subsequently, the carbides were extracted by dissolution of the f c c phase in a mixture of bromine (10 vol %) in methanol, then diffraction patterns on extracted carbides were obtained in a Guinier camera, using chromium radiation. Some very pure silicon added to the carbides was used as standard.

Specimens for electronmicroscopy were prepared by electropolishing discs using a jetting technique with 20% perchloric acid, 10% glycerol in ethanol with 20 V applied voltage. Acceptable specimens thus prepared were examined in a JEM 100 B microscope. Carbon extracted replicas were also observed by transmission electron miscroscopy (TEM).

3. Results

3.1. Sintered alloys

3.1.1. Morphology of the microstructure

As previously mentioned, microstructures observed after sub-solidus sintering were very different depending on the grain size of the initial powder. Fig. 1 compares the optical micrographs of the samples obtained by casting or sintering of the two grain size powders.

The small size powder ($< 36\,\mu$m) provides a very thin dispersion of precipitates in the matrix

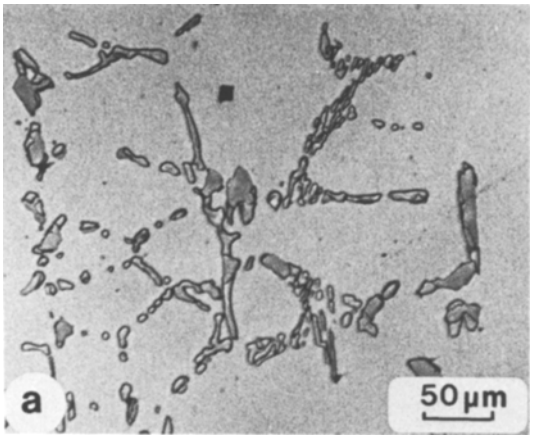

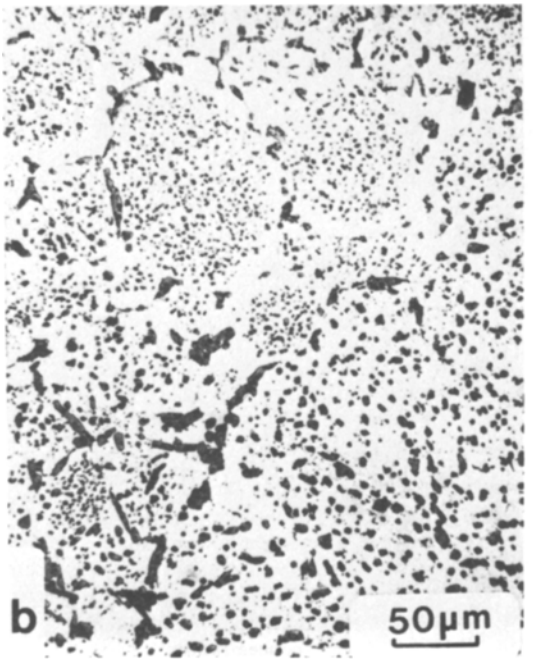

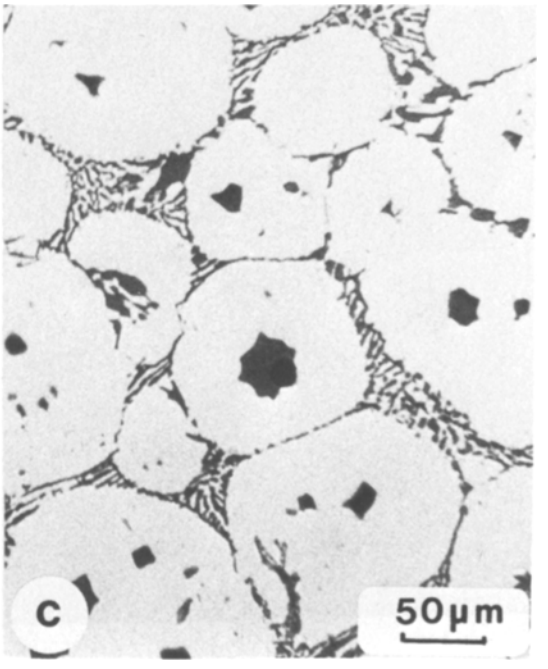

Figure 1 Optical micrographs comparing the microstructures of (a) an as-cast sample, (b) a Type I structure obtained by liquid phase sintering of $< 36\,\mu$m powder and (c) Type II structure obtained by liquid phase sintering of $< 500\,\mu$m powder.

(Type I structure). However, a structural arrangement begins to appear in which cells in the range 30 to 150 μm are surrounded by rather large carbides (20 to 70 μm in length). An important precipitation of smaller particles (< 5 μm) takes place inside the cells. No grain boundary can be easily detected by optical microscopy.

The mixed size powder (< 500 μm) leads to a clearly cellular structure (Type II). The cell size is in the range 40 to 250 μm, it can be noted that no cells larger than about 300 μm are found. Cells are surrounded by eutectic zones consisting of elongated carbide precipitates and the matrix. In the centre of numerous cells, jagged-outline islands are observed. The size of these islands is in the range 5 to 70 μm, but their mean value is about 30 μm. Without any chemical etching, these islands appear to be a single phase, however, they are strongly darkened by the Murakami reagent which also reveals a multi-phase structure. This extremely fine structure, easily observed by photoemission electron microscopy is shown in Fig. 2; it seems to contain two phases of about the same dimension (0.1 to 0.6 μm). However, at higher magnification, a SEM micrograph (Fig. 3) shows a structure which could correspond to three constitutive phases.

A large number of observations carried out on several samples establish that no grain boundary ends at any part of these islands; also it is found that a small hole is present in each island. Due to their special shape and their constant overall composition, these islands were called "star-phase" though they did not consist of a single phase. Such

Figure 2 Photoemission electron micrograph of the star phase. The darker part of the matrix corresponds to a higher W concentration.

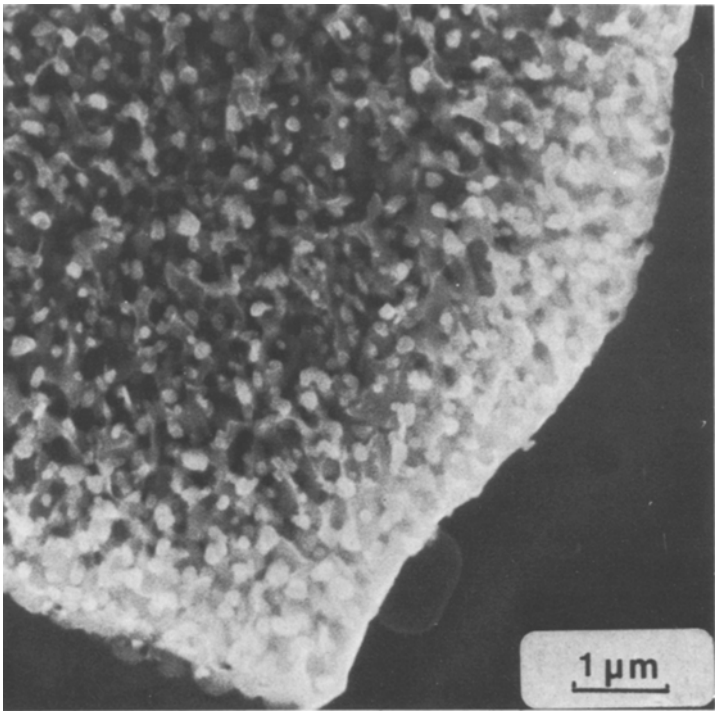

Figure 3 Scanning electron micrograph of the star phase.

a microstructure has been already mentioned by Clemow and Daniell [6], Thorley [7] and Clauss *et al.* [8] on superalloys based on Co–Cr–Mo, it has been recently described by Kilner *et al.* [9] on Vitallium and Vinertia (Co–Cr–Mo–C).

3.1.2. Phase composition

Owing to its very thin structure, the microanalysis of Type I material was difficult and only the compositions of the matrix and larger precipitates were measured. In Type II material the matrix and precipitates were easier to analyse owing to their larger size. However, the very thin morphology of the star phase only permitted the overall composition to be measured using an unfocussed microprobe. This composition was found to be approximately constant for all the different islands.

The results of the phase composition determinations are presented in Table II. In order to get a valid comparison of the small differences in content of the several elements between the two types of materials, the corrected values (wt %) are taken into account. Only the evolution of the main elements Co, Cr, W and C in M_7C_3 are considered, the possible change in content of the minor elements, Si, Fe and C, in the matrix being not significant.

For Type I, the results indicate that the compositions of the phases are very close to those

TABLE II Phase composition results for sintered materials

Element	Type I (starting powder size < 36 µm)				Type II (starting powder size < 500 µm)					
	Co phase (S_2)		M_7C_3 (C_2)		Co phase (S_1)		M_7C_3 (C_1)		Star phase (Y)	
	X*	X_A†	X	X_A	X	X_A	X	X_A	X	X_A
C	0.03	0.15	8.86	30.10	0.15	0.75	9.39	31.63	6.31	24.37
Si	1.32	2.75	0	0	1.16	2.40	0	0	0.60	0.99
Fe	0.27	0.28	0.09	0.07	0.28	0.29	0.10	0.07	0.17	0.14
Cr	24.06	27.09	76.98	60.38	24.88	27.78	74.75	58.17	49.25	43.9
Co	68.70	68.26	12.78	8.85	68.72	67.67	13.32	9.15	36.20	28.47
W	4.57	1.46	2.71	0.60	3.56	1.12	4.44	0.98	8.47	2.13

*X = corrected values (wt %).
†X_A = at %.

determined under thermodynamic equilibrium conditions for the solidus temperature.

For Type II, the fcc solid solution exhibits a slight increase in the Cr content and a marked decrease in the W level, while the Co content does not change. For the precipitates the opposite trend is noted, with decreasing Cr and increasing W contents; moreover a slight but significant increase of the C level is reported. The main feature regarding the equilibrium conditions is the significant depletion of W in the solid solution which represents more than 20% of the total W content; this lack is balanced by the high W concentration measured in the star phase which also corresponds to a very high C level. Moreover, segregations are detected on the edge of the cells and in the serrated matrix located around the star-phase islands. Due to the small size of these parts a quantitative analysis is difficult; however, from count results and concentration profiles, they are found to correspond to slightly higher Co, higher W and lower Cr levels; the overall effect appears as a decrease of the (Cr + W) atomic fraction.

From these results, the incomplete diffusion of W seems to be responsible for the formation of the star phase.

3.1.3. Crystal structures

From the patterns obtained by X-ray diffraction, the precipitates extracted from the two structure types, are found to be mainly the M_7C_3 carbide, this result is in agreement with the phase composition measurements. By TEM, the analysis of selected-area diffraction patterns leads to the same conclusion.

The diffraction pattern is very streaky. As mentioned by Dyson *et al.* [10], these streaks are the result of faults in the crystal structure in planes perpendicular to (0 0.1). In the X-ray diffraction patterns, some extra reflections could be attributed to the $M_{12}C$ phase according to the crystal structure data published by Pollock and Stadelmaier [11] and Mary [12]. These reflections, which are not observed on all of the samples, are only found in Type II material; also in this material, a very small amount of $M_{23}C_6$ is detected.

By X-ray diffraction of the two types of bulk specimen, the matrix is confirmed as the Co-base

Figure 4 Bright-field electron micrograph of the Type II matrix.

TABLE III X-ray results; lattice parameters of M_7C_3 and Co phase

Phase	Structure type	Lattice parameters (nm)
M_7C_3	hcp P 31 C	$a = 1.403$ $c = 0.450$
$M_{23}C_6$	fcc Fm 3m	$a = 1.0627$
γ-Co phase	fcc Fm 3m	$a = 0.3573$

f c c solid solution, with some ϵ hexagonal phase. Electron microscopical examination of a Type II specimen shows this transformed h c p phase appearing as mosaics in the matrix (see Fig. 4). For the main phases, the lattice parameters calculated from the diffraction patterns are given in Table III.

3.2. Aged alloys

3.2.1. Microstructure after ageing

In order to reach a better understanding of the star phase formation, ageings were effected on sintered samples at several temperatures. First of all, a Type II sample was slowly heated up to 900° C in a photoemission microscope (PEM). *In situ* observations evidenced an important precipitation from about 650° C, however, no rapid evolution appeared for the star phase. In addition samples annealed at higher temperatures (1230 and 1150° C) were studied.

3.2.1.1. In-situ observations. As shown in Fig. 5a, at room temperature, an orientation contrast can be observed inside some cells of the f c c phase. On heating above 650° C, a large number of streaks in the matrix appeared. These streaks formed several groups of parallel lines intersecting at well-defined angles, see Fig. 5b. A change of orientation of the matrix is seen to correspond to a change of orientation of the streaks.

The rather low magnification used in the high temperature microscope did not permit monitoring of the evolution of the star phase. More information was obtained by SEM and TEM observations of the same sample after heating up to 900° C for two hours in the Metioscope and slow cooling. As shown by the SEM micrographs, Fig. 6a presents the general aspect of the microstructure, Fig. 6b reveals the intense precipitation inside the matrix cells and Fig. 6c shows the new aspect of the star phase which consists of three distinct phases. Following energy dispersive analysis by X-ray (EDAX) semiquantitative investigation, two of these phases seem to be the matrix and the

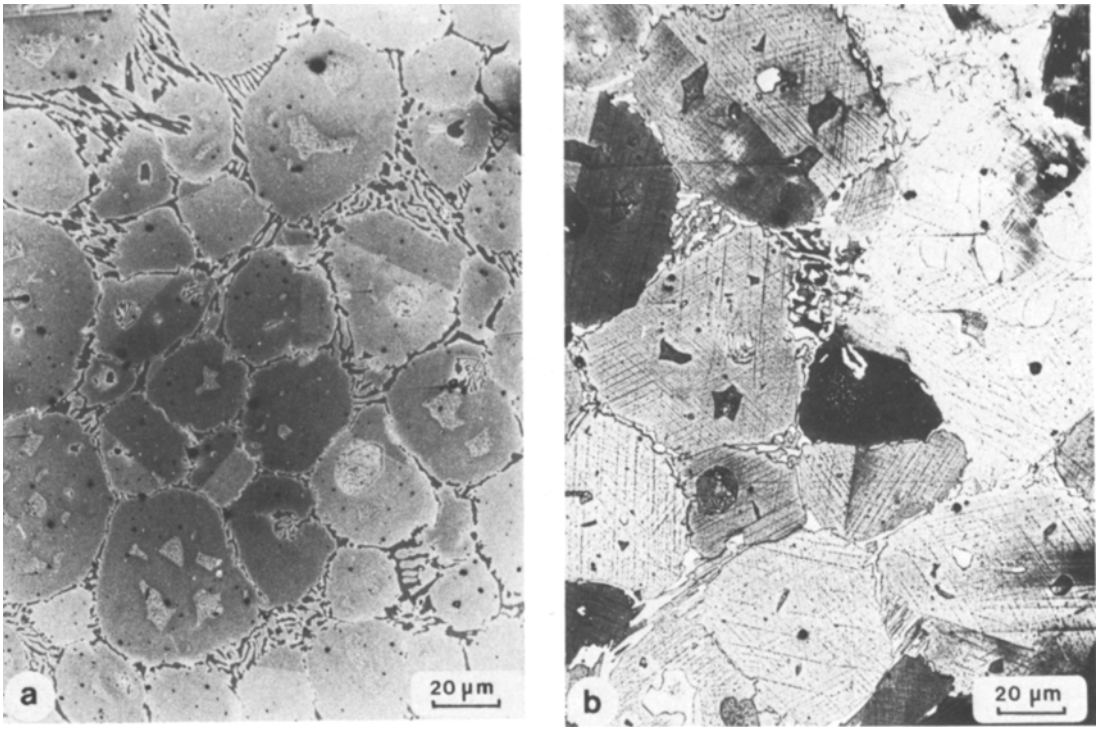

Figure 5 PEM *in-situ* observations of Type II structures, at (a) room temperature and (b) 650° C.

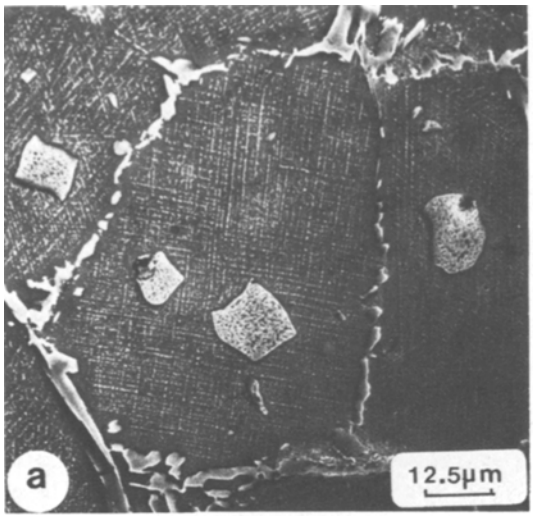

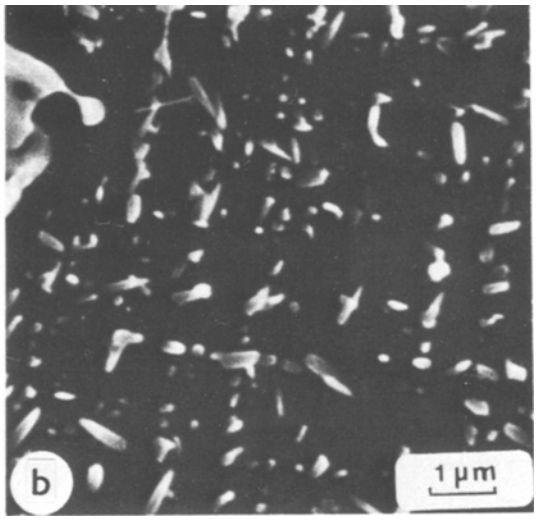

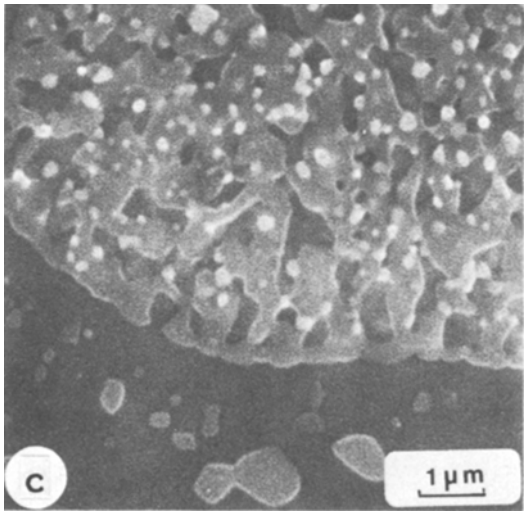

Figure 6 SEM observations of the sample aged at 900° C for 2 h showing (a) general view, (b) matrix precipitation and (c) star phase. Owing to strong chemical etching of the sample, contrast is mainly due to topography and cannot be related to atomic number difference.

M_7C_3 type carbide, and the third phase, which is the lightest, is shown to be the richest in W. This phase is present in a very small quantity compared with the M_7C_3 carbide and the embedded matrix.

On the same specimen, more details on the various phases were obtained by electron microscopy. As shown in Fig. 7, the matrix is f c c with very thin lamellae (see Fig. 8a). These thin lamellae produce additional spots in the diffraction patterns indexed according to the ϵ Co phase (Fig. 7b, c). The dark-field image of this ϵ Co phase is shown in Fig. 7d. The orientation relationship between the f c c and h c p structure is characteristic, i.e.,

$$(1\,1\,1)_{fcc} \parallel (0\,0.1)_{hcp}$$
$$[0\,\bar{1}\,1]_{fcc} \parallel [1\,1.0]_{hcp}. \quad (1)$$

The streaking in the diffraction spots along the ⟨1 1 1⟩ directions results from the small dimensions of the h c p lamellae along these directions.

In addition, the aged alloy shows precipitates of $M_{23}C_6$ in the matrix, see Fig. 8a. These particles are coherent with the matrix and exhibit the classical orientation relationship for cubic systems, i.e.,

$$[0\,0\,1]_M \parallel [0\,0\,1]_{M_{23}C_6}$$
$$(0\,1\,0)_M \parallel (0\,1\,0)_{M_{23}C_6}. \quad (2)$$

These particles appear as needles and are related to the striation which is visible on the PEM as well as on the scanning electron micrographs (see Figs 5 and 6). Some particles of M_7C_3 appear also in the matrix, but they do not present any particular form or orientation relationship with the matrix.

The star phase appears in electron microscopy as round cells (0.5 to 1 μm in diameter). Its spheroidal structure is very different from the geometrical forms of M_7C_3 carbides nucleated in the matrix as shown in Fig. 8. Some darker phases inside the round cells of the star phase have been observed, which can be related to the light phase seen in the SEM (see Fig. 6) which was shown to contain a high W level. According to the results of X-ray diffraction, this dark phase could correspond to the small amount of $M_{12}C$ detected in

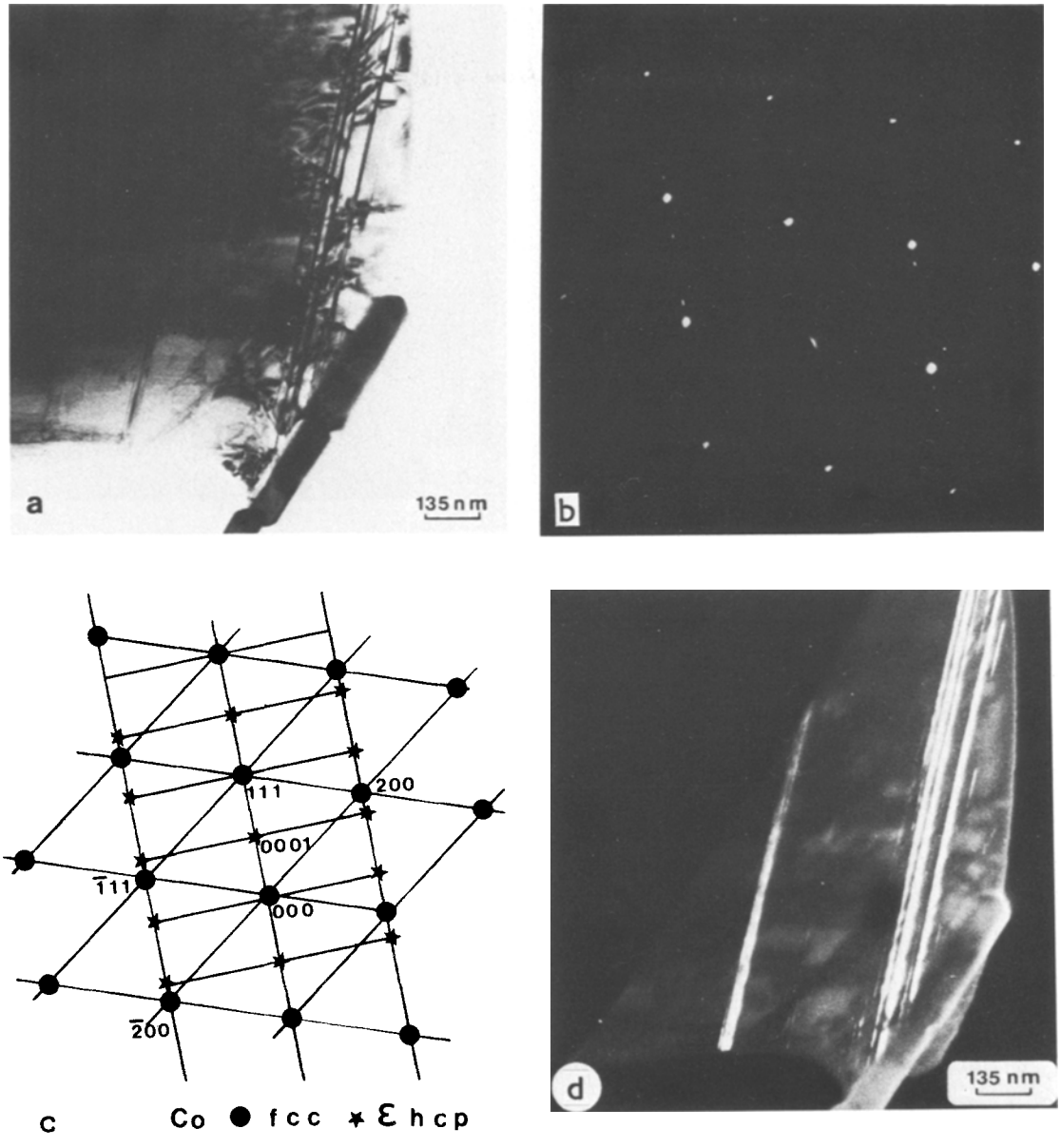

Figure 7 TEM observations of the sample aged at 900° C for 2 h showing (a) bright-field, (b) diffraction pattern, (c) identification of the reflections of the diffraction pattern and (d) dark-field on ϵ phase spots.

the patterns. Effectively, $M_{12}C$ is generally based on Co_6W_6C and must contain a large quantity of W. Another possibility concerns the M_6C phase, which has a crystal structure very similar to $M_{12}C$. Its composition can evolve from Co_3W_3C to Co_2W_4C [11, 12]. It was found recently [13] that its lattice parameter depends on its W and Si contents, and can be very close to the lattice parameter of $M_{12}C$. The two phases can be easily mistaken. The two other phases present in the star phase are identified unambiguously by electron diffraction as M_7C_3 and the f c c matrix.

3.2.1.2. High temperature ageing. Sintered samples were aged for 4 h at 1150° C. The optical micrographs obtained are shown on Fig. 9. For Type I as well as for Type II structure, no appreciable change of the cell size was observed, however,

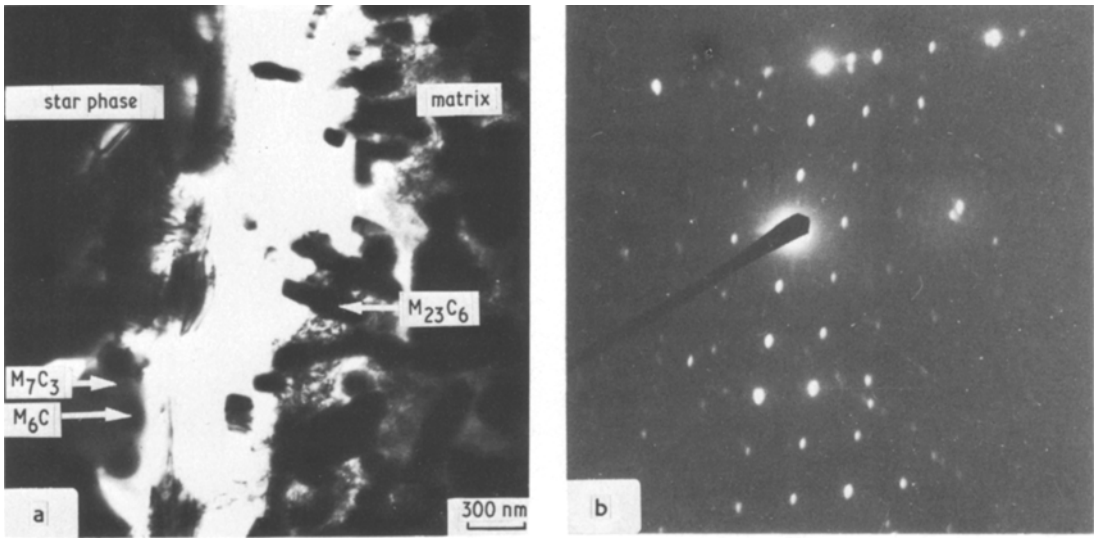

Figure 8 (a) Bright-field micrograph of the boundary between the matrix, star phase and matrix precipitates and (b) Diffraction pattern of the matrix [1 1 0] and $M_{23}C_6$ precipitates. The brightest spots are related to the matrix.

the coalescence of the small carbides could easily be measured. For the large carbides, a thickening was noted without an increase in length. The oriented precipitation of $M_{23}C_6$ in the matrix appeared clearly in Type II and could also be detected in Type I. The mean size of the star phase did not change but its outline became more regular and its microstructure coarsened drastically.

The composition of the main phases, i.e., matrix, M_7C_3 and star phase, are reported in

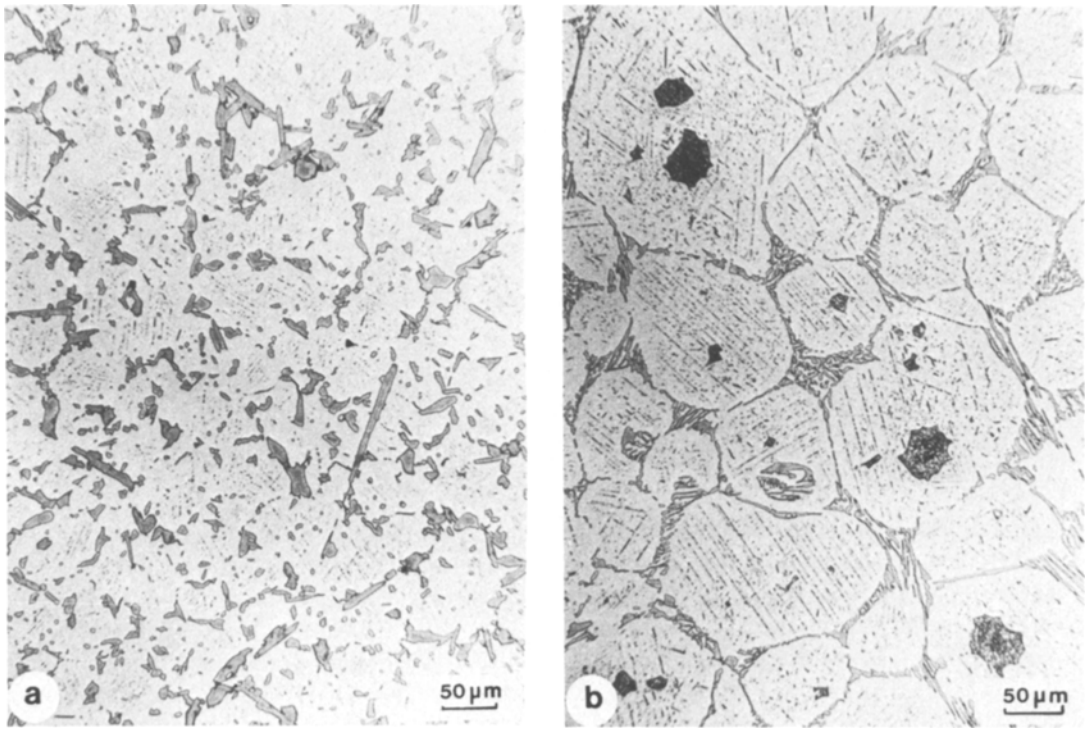

Figure 9 Optical micrographs of the samples aged at 1150° C for 4 h showing (a) Type I structure and (b) Type II structure.

TABLE IV Phase composition results for aged materials

Element	Type I (starting powder size < 36 μm)				Type II (starting powder size < 500 μm)					
	Co phase		M_7C_3		Co phase		M_7C_3		Star phase	
	X*	X_A†	X	X_A	X	X_A	X	X_A	X	X_A
C	0.22	1.06	8.36	28.93	0.19	0.91	8.49	29.47	5.61	21.5
Si	1.23	2.55	0	0	1.18	2.45	0	0	0.48	0.79
Fe	0.29	0.30	0.09	0.07	0.29	0.30	0.10	0.08	0.18	0.15
Cr	23.45	26.28	76.88	61.46	23.35	26.20	75.16	60.29	52.04	46.07
Co	69.15	68.38	12.70	8.96	69.69	68.98	12.97	9.18	38.55	30.11
W	4.49	1.42	2.58	0.58	3.63	1.15	4.35	0.99	5.46	1.37

*X = corrected values (wt%).
†X_A = at%.

Table IV. For the sintered state, the evolution of the fcc matrix is small. Only a slight increase in Co and decrease in Cr are observed for the two types of materials. As for the M_7C_3 carbide, the main change is a small decrease in the C content. The only clear change concerns the star phase for which the C and W contents decrease when the Co and Cr levels increase. No TEM observation was effected on thin slices of these specimens, consequently it is not possible to draw any conclusions about the presence of the hcp Co phase in this sample.

It can be seen that ageing at 1150° C for 4 h results mainly in the formation of $M_{23}C_6$ which could be related to the Cr desaturation of the matrix. This precipitation is generally attributed to a change of the limit solubility of C in the solid solution. In the present case, the composition evolution of M_7C_3 might also provide some C for this precipitation. For Type II structure the results clearly show that the annealing time is not long enough to promote the complete diffusion of the W segregated in the star phase. However, the minor phase previously observed by SEM, in the star phase, is no longer found after this long ageing (see Fig. 10), so that the star phase appears to consist only of M_7C_3 and matrix. The disappearance of this phase indicates that it is in a non-equilibrium state in this material.

4. Discussion

The supersolidus sintering of prealloyed powders

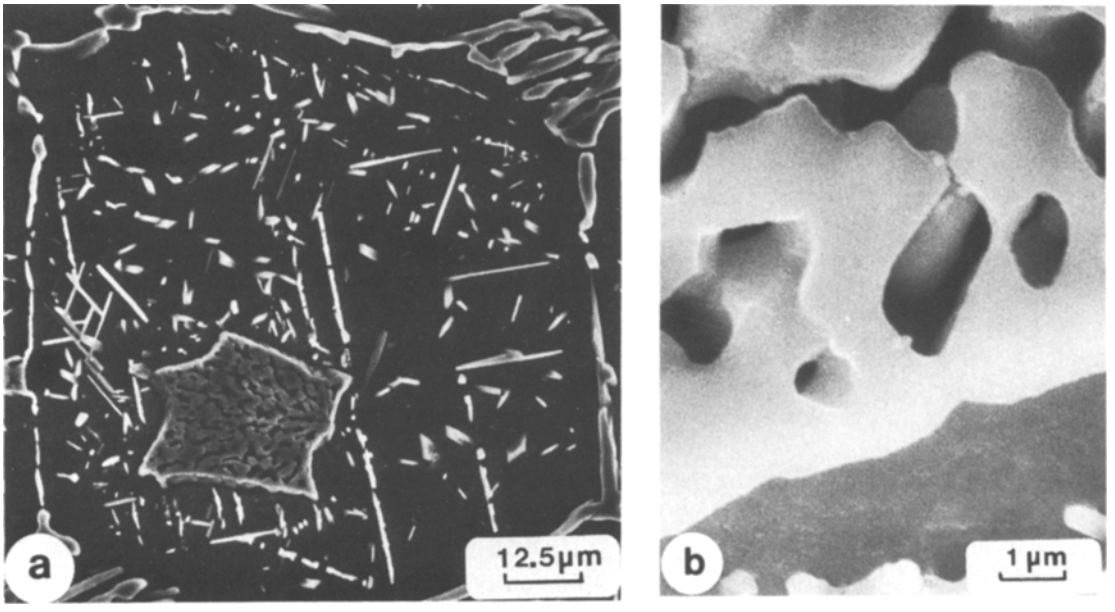

Figure 10 SEM observation of the sample aged at 1150° C for 4 h showing (a) general view and (b) star phase. The marked contrast is mainly due to the effects of chemical etching and cannot be related to atomic number difference.

of Stellite 6 type alloy leads to microstructures which are very different depending on the grain size of the initial powder. In the present work, no attempt was made to study the densification mechanisms involved in this partial melting process. However, taking into account the results obtained by Huppmann [14] and Petzow [15], for the elementary mechanisms of liquid phase sintering, an attempt can be made to explain the formation of these two types of structure from an initial state which was shown [5] to correspond to a microcrystalline morphology for the thinner powder ($< 50\,\mu m$) and a dendritic structure for the coarse beads ($> 50\,\mu m$).

4.1. Type I structure

The liquid phase sintering of the thin powder ($< 36\,\mu m$) provides a material consisting of a uniform dispersion of M_7C_3 carbide in an austenitic Co–Cr matrix containing some h c p phase. The composition of the phases is very close to the compositions determined under equilibrium conditions in the sintering temperature range; consequently, it can be assumed that the microstructure observed is formed during the step when the solid grains coarsening occurs by Ostwald ripening. This step was defined by Huppmann and Petzow [14] as the last stage of sintering; it corresponds to the normal grain growth which takes place as chemical equilibrium is reached. The two-phase microcrystalline morphology of the thinner initial powder, which exhibits a coarsening of M_7C_3 as well as the Co phase on sintering, appears to correspond to a heating in a three-phase domain where some liquid is present with M_7C_3 and Co. According to the equilibria results, this domain might be stable only up to $1280 \pm 5^\circ$ C while sintering is performed at about $1295 \pm 5^\circ$ C. This slight discrepancy might be explained by the experimental conditions of temperature measurements which are not the same in each case. The microstructural observations were performed only after complete sintering: they did not enable the present authors to explain the beginning of cell arrangement and specifically to relate it to the initial size of the beads.

Despite the coarsening during sintering, the size of the solid grains is small, therefore the solid surface is large and the liquid phase forms a thin layer around the solid grains. On cooling, the liquid solidifies on a eutectic line ($Co + M_7C_3$). Owing to the small local amount of liquid, each of the eutectic phases formed by cooling, freezes on the pre-existing solid phases, therefore the usual eutectic morphology is not observed. The small amount of h c p Co phase is probably formed during the cooling of the sintered samples. The ageing of these alloys produces a rather slight coarsening of the carbides; it induces an important precipitation of $M_{23}C_6$ carbide.

4.2. Type II structure

The liquid phase sintering of mixed size powder provides a cellular structure. The cells of the f c c Co phase, in which some h c p phase is present, are surrounded by a continuous ($Co + M_7C_3$) eutectic mixture. Inside the cells, numerous islands with jagged outline and very fine structure are present. This material does not correspond to the thermodynamic state previously determined. The W level, which is lower in the Co phase than in the equilibrium matrix, is rather high in the star phase, and the star phase is never detected in the equilibrium structure.

The star phase appears to correspond to a liquid phase at the sintering temperature. This assumption is deduced from the following observations:

(a) The very special serrated boundary is generally found when a liquid phase, resulting from a high temperature treatment, is rapidly cooled at low temperature. Such behaviour has been already mentioned by several authors [16, 17].

(b) The presence of a small hole in most of the star phase islands can be attributed to a solidification hole.

(c) The ultrafine spheroidal morphology, as observed in the star phase, is generally related to the solidification of a strongly undercooled liquid phase [18].

(d) An incipient melting is found to occur, for similar star phases in Co–Cr–Mo alloys, by several authors [6–9].

Moreover, no grain boundary ends at any part of the star phase and the composition of the several islands is found to be constant.

Comparing the initial state, which consists of a mixture of thin cellular and coarse dendritic beads, with the 40 to $250\,\mu m$ cell assembly observed after sintering, and using the scheme described by Huppmann and Petzow [14], it can be expected that the heating would produce the following phenomena:

(i) Melting of the interdendritic parts and subsequent fragmentation of the coarser cells.

(ii) Dissolution of the smallest grains of Co phase and reprecipitation on the original dendrites.

(iii) Coarsening of the dendrites.

No observations having been performed before complete sintering, it is not possible to correlate the cell formation with the initial bead size. However, at the sintering temperature, the material appears as a large amount of Co cells surrounded by the liquid phase. Inside the cells, numerous liquid pockets are trapped by the coarsening of dendrite neighbouring arms. As regards the equilibrium results, the material is maintained in the metastable (Co + liquid) domain by incomplete diffusion of W in the solid phase.

4.3. Cooling behaviour and star phase formation

Due to the mixed size of the starting powder, a large range of initial porosity size might be found. Consequently, when a liquid phase forms on heating, a rather irregular distribution of liquid can be expected, even if attenuated by the particle rearrangement which takes place during the first step of liquid phase sintering [15]. Such a distribution is confirmed by the micrograph (Fig. 1c) which shows the Co cells separated by large areas as well as thin layers of eutectic structure, and star-phase islands. The eutectic morphology results from the solidification of the large size liquid parts, the elongated carbides come from the freezing of liquid layers squeezed between Co cells, and the star phase, results from the liquid pockets enclosed inside the cells. It can be noted that such liquid pockets are very similar to closed pores formed in the case of solid state sintering: no communication exists with the other liquid parts and grain boundary diffusion is not possible.

In order to explain the solidification behaviour, the material can be regarded as composed of two systems behaving independently, the first one consisting of Co phase and the surrounding liquid phase and the second one corresponding to the isolated liquid islands. To a first approximation, the liquid phase composition can be assumed to be the same for the two systems. As regards the overall composition, C, of the starting material, the first system, System A, corresponds to a smaller liquid proportion while the second system, System B, consists of a separate part of the same liquid. Obviously the sum of the two systems is equivalent to the overall composition, C.

The actual freezing can then be deduced from the solidification path determined under equilibrium conditions [4] for the composition, C. Freezing takes place in two steps shown in Fig. 11, first, crystallization of Co–Cr solid solution with simultaneous increasing of the W, Cr and C levels in the liquid, and then eutectic solidification of the liquid as M_7C_3 + Co–Cr phase mixture. During freezing, the composition of the Co phase changes from S to S_1 during the first step, from S_1 to S_2 during the second step; the liquid composition evolves from S_1 to X in the first step, then along the eutectic line XX'.

Taking System A, its cooling evolution has to follow the same path. Owing to the smaller liquid fraction, a smaller amount of eutectic has to form. Regarding the equilibrium conditions, the initial lack of W in the Co cells and the rapid cooling of the specimens which prevents solid state diffusion, will induce an important segregation of the main alloying elements (W, Cr and C) in the eutectic mixture.

For the system having composition B, as already pointed out, its isolated location prevents any grain boundary diffusion, consequently, the movement of solute atoms is due to volume diffusion only. Taking into account previous results, the solidification of System B can be assumed to occur in the following way. The Co phase solidifies around the liquid pockets exhibiting a dendritic morphology, as the temperature decreases, the composition of the interface solid layer keeps in equilibrium with the liquid and evolves as SS_1S_2. During the rapid cooling, the very sluggish diffusion does not permit any homogenization of the solid phase and the solute concentration in the liquid reaches supersaturation; the liquid phase is retained by supersaturation at a temperature lower than the eutectic line. As observed in a binary system, in the case of undercooling, the liquid composition evolves on the prolongation of the liquidus surface keeping a metastable equilibrium with the solid phase. According to the results of several authors [19, 20] on the Co–Cr–C system, in this composition range, the liquidus surface is flat and the temperature gap between liquidus and solidus is wide so it can be expected that the liquid can reach an important degree of supersaturation for a rather small undercooling.

Examining the composition results carefully (Table II), a fair agreement is observed with this freezing scheme as presented in Fig. 11. For

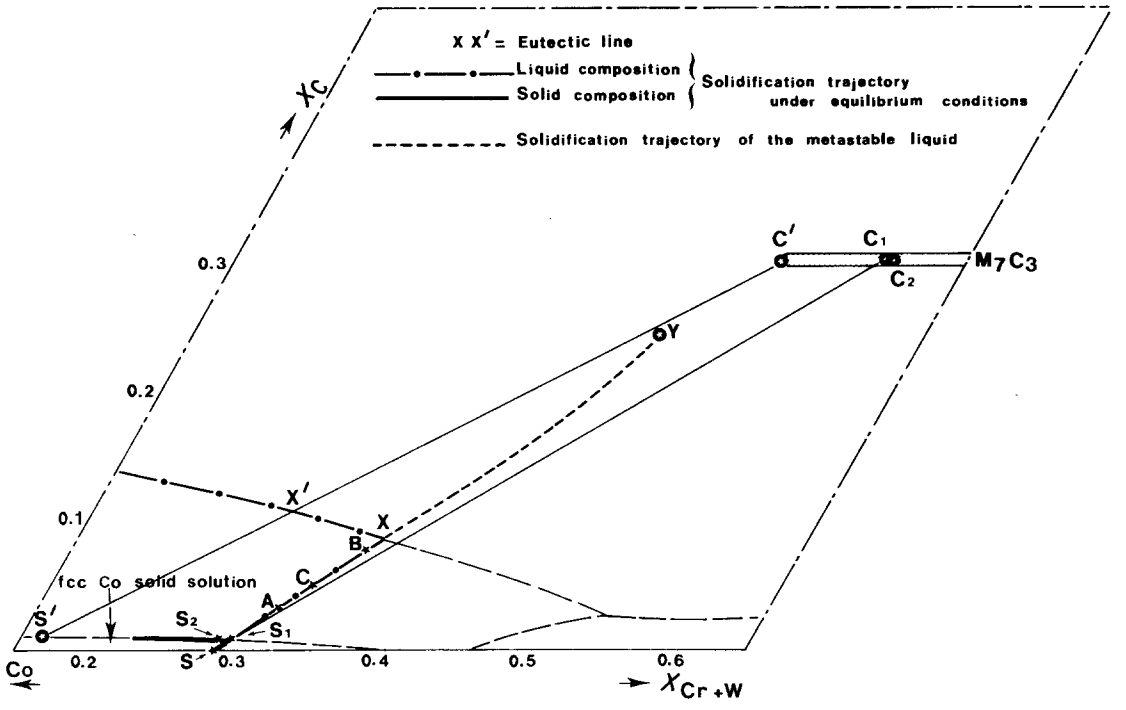

Figure 11 Pseudo-ternary representation of the solidification behaviour of PY-250 Type II material. X_C and X_{Cr+W} are the atomic fractions of C and Cr + W respectively. S_1, C_1 and Y are the compositions of Co matrix, M_7C_3 and star phase in Type II material, and S_2 and C_2 are the compositions of Co matrix and M_7C_3 in Type I material. S'–C' is the limiting tie line of the Co–M_7C_3 domain in the Co–Cr–C system.

System A the Co cell composition corresponds to S_1; in the eutectic part, the Co phase composition, richer in W, poorer in Cr, is in the S_2 direction. For System B, the concentration profiles of Co, W and Cr also indicate an evolution in the direction of S_2 for the dendritic layer frozen around the liquid pockets, while the liquid phase concentrates up to Y. It has to be noted that this pseudo-ternary representation shows an overall evolution which corresponds to a decrease in (Cr + W) and does not point out the increased W content.

Another point to be clarified is the limit composition, Y, reached by the liquid. It could be thought that the liquid was maintained by supersaturation and the interfacial energy created by the important dendritic surface. Due to the unfocussed microprobe analysis, star-phase islands smaller than 10 μm were never analysed. However, for islands of very different sizes, larger than 10 μm, a remarkable consistency of composition is observed. Consequently, the interface effect does not seem to contribute appreciably to the stabilization of the supersaturated liquid and the limit concentration seems to depend mainly on the phase domain in the pseudo-ternary Co–(Cr + W)–C system.

This assumption is ascertained by the fact that the composition, Y, is located close to the tieline plotted by Sahm *et al.* [21] as the limit of the Co + M_7C_3 domain in the Co–Cr–C system, since a similar behaviour was found for the pseudo-ternary alloys.

At this point, a further evolution of the liquid phase is no longer possible and massive solidification takes place in the form of a globular mixture of Co phase, M_7C_3 and some M_6C (or $M_{12}C$). Owing to its very high W level, the solidification behaviour of the Y composition can no longer be explained by reference to the pseudo-ternary Co–(Cr + W)–C system. The literature data published on the quaternary system by Knotek *et al.* [22] do not concern the C level corresponding to Y. It is only possible to note that the W-rich phase (M_6C or $M_{12}C$) is not stable for the overall composition of the alloy, it disappears on high temperature annealing, by diffusion of segregated W. At this temperature, the phases present in the material are M_7C_3, $M_{23}C_6$ and the Co phase, as

indicated by Knotek *et al.* [22] for about the same concentration range.

5. Conclusion

Liquid phase sintering of prealloyed powders of Co base alloys provides microstructures which can be very different depending on the initial powder size. The comparison of the sintered and initial states indicates this difference to be mainly related to the initial morphology of the powders.

The finest powders are shown to form a dispersion of M_7C_3 in a Co phase matrix corresponding to the thermodynamic phase equilibria.

The mixed size powders create a cellular structure in which islands of very fine structure are present as well as M_7C_3 and Co phase. The formation of these islands can be attributed to the massive solidification of a liquid supersaturated in W, Cr, C. The high degree of supersaturation is related to the lack of diffusion of solutes in the solid phase.

The solidification of these materials can be explained by a Co–(Cr + W)–C pseudo-ternary representation, however, in this case, the overall effect of (Cr + W) does not sufficiently emphasize the prevailing segregation effect of W.

References

1. H. W. SHARP, *Welding J.* **25** (1946) 936.
2. A. J. HICKL, *J. Met.* **6** (1980) 12.
3. W. L. SILENCE, *J. Lubr. Tech. Trans. ASME* **100** (1978) 428.
4. C. GUYARD, A. BARBANGELO, C. H. ALLIBERT and J. DRIOLE, *J. Mater. Sci.* **16** (1981) 604.
5. C. GUYARD, C. H. ALLIBERT, J. DRIOLE and G. RAISSON, *Sci. Sintering* **13** (3) (1981) 149.
6. A. J. T. CLEMOW and B. L. DANIELL, *J. Biomed. Mater. Res.* **13** (1979) 265.
7. S. THORLEY, Sulzer Report No 1048 (1974).
8. F. J. CLAUSS, F. B. GARRETT and J. W. WEETON, N.A.C.A. 1955. TN 3512.
9. T. KILNER, R. PILLIAR, G. WEATHERLY and C. H. ALLIBERT, *J. Biomed. Mater. Res.*, in press.
10. D. Y. DYSON and K. W. ANDREWS, *J. Iron Steel Inst.* (1968) 208.
11. C. B. POLLOCK and H. H. STADELMAIER, *Met. Trans.* (1970) 767.
12. Y. MARY, *Rev. Chim. Minér.* **6** (1969) 585.
13. M. DURAND-CHARRE, S. HAMAR-THIBAULT and B. ANDRIES, *Rev. Métall. Paris* (1981) 321.
14. W. J. HUPPMANN and G. PETZOW, "Materials Science Research" Vol. 13 (Plenum Press, New York, 1980) p. 189.
15. G. PETZOW and W. J. HUPPMANN, *Z. Metallk.* **67** (1976) 579.
16. ASM Metals Hand Book, 8th Ed. Vol. 7, Plate 2146 (American Society for Metals, Metals Park, Ohio) p. 260.
17. H. BILONI, G. F. BOLLING and G. S. COLE, *Trans. AIME* **230** (1966) 930.
18. H. B. KEAR, P. R. HOLIDAY and A. R. COX, *Met. Trans.* **10A** (1979) 191.
19. E. R. THOMPSON and F. D. LEMKEY, *ibid.* **1** (1970) 2799.
20. P. R. SAHM and D. Y. WATT, *ibid.* **2** (1971) 1260.
21. P. R. SAHM, M. LORENZ, W. HUGI and V. FRÜHAUF, *ibid.* **3** (1972) 1022.
22. O. KNOTEK, H. SEIFAHRT and R. KIEFFER, *Arch. Einsenhutten* **39** (1968) 869.

Received 6 July
and accepted 22 July 1981